Articles in PresS. Am J Physiol Renal Physiol (October 26, 2016). doi:10.1152/ajprenal.00143.2016

A Kidney-selective Biopolymer for Targeted Drug Delivery

Gene L. Bidwell, III [1,2*], Fakhri Mahdi [1], Qingmei Shao [1], Omar C. Logue [1], Jamarius P. Waller [1], Caleb Reese [3], and Alejandro R. Chade [4]

1. Department of Neurology, University Of Mississippi Medical Center, Jackson, MS 39216
2. Department of Biochemistry, University Of Mississippi Medical Center, Jackson, MS 39216
3. Belhaven University, Jackson, MS 39202
4. Departments of Physiology and Biophysics, Medicine, and Radiology, University Of Mississippi Medical Center, Jackson, MS 39216

Author Contributions: FM, QS, OCL, JPW, and CR collected and analyzed data and contributed to the writing of the manuscript. ARC and GLB designed the study, performed experiments, analyzed data, and drafted, edited, and approved the final version of the manuscript.

Running Head: A kidney-targeted biopolymer for drug delivery

*** Address for Correspondence:**

Gene L. Bidwell, III, Ph.D.

Department of Neurology

University of Mississippi Medical Center

2500 North State Street

Jackson, MS 39216

gbidwell@umc.edu

Abstract.

Improving drug delivery to the kidney using renal-targeted therapeutics is a promising but under-developed area. We aimed to develop a kidney-targeting construct for renal-specific drug delivery. Elastin-like polypeptides (ELPs) are non-immunogenic protein-based carriers that can stabilize attached small molecule and peptide therapeutics. We modified ELP at its N-terminus with a cyclic, seven amino acid kidney-targeting peptide (KTP) and at its C-terminus with a cysteine residue for tracer conjugation. Comparative *in vivo* pharmacokinetics and biodistribution in rat and swine models and *in vitro* cell binding studies using human renal cells were performed. KTP-ELP had longer plasma half-life than ELP in both animal models and similarly accumulated in kidneys at levels 5-fold higher than untargeted ELP, showing renal levels 15- to over 150-fold higher than in other major organs. Renal fluorescence histology demonstrated high accumulation of KTP-ELP in proximal tubules and vascular endothelium. Furthermore, a 14-day infusion of a high dose of ELP or KTP-ELP did not affect body weight, glomerular filtration rate, albuminuria, or induce renal tissue damage compared to saline-treated controls. *In vitro* experiments showed higher binding of KTP-ELP to human podocytes, proximal tubule epithelial, and glomerular microvascular endothelial cells than untargeted ELP. These results show the high renal selectivity of KTP-ELP, support the notion that the construct is not species specific, and demonstrate that it does not induce acute renal toxicity. The plasticity of ELP for attachment of any class of therapeutics unlocks the possibility of applying ELP technology for targeted treatment of renal disease in future studies.

Keywords. Elastin-like Polypeptide, kidney targeting peptide, drug delivery, renal disease, biopolymer

Introduction.

Renal disease represents a growing market for drug development. The incidence of chronic kidney disease (CKD) has been steadily increasing for the past two decades in patients 65 and older (39), and an estimated 31 million people in the United States have CKD (1). In turn, the incidence of end stage renal disease has climbed to a rate of 350 per million in the US population (39). This highlights the importance of not only developing new drugs for renal disease, but also new strategies improving drug delivery to the kidney and, if possible, targeting therapeutics to the appropriate cell type.

Previous studies focused on kidney-selective drug delivery by utilizing passive targeting of endogenous low molecular weight proteins (LMWPs) that naturally accumulate in the kidney (55), such as lysozyme, immunoglobulin light chain, or insulin. LMWPs can be fused to therapeutics to increase their renal accumulation (14, 23, 55), but tend to be filtered and taken up by tubular cells (20, 54). Therefore, this strategy may be limited to certain pathologies of proximal tubular epithelial cells (55). Potential alternatives are to utilize glycoconjugates to target drugs to specific renal membrane receptors (25, 50) or to fuse therapeutics to nanoparticle carriers that are too large to be filtered and may target pre- and glomerular cells (29, 57). However, depending on their makeup, nanoparticles technology can be limited by cytotoxicity (24, 35). Other avenues for renal targeting can also be paved by fusing drugs to ligands for receptors highly expressed in the kidney, such as a galectin-3 targeting peptide (56) that has been tested for renally-targeted delivery of captopril (16). However, to date, none of these strategies are used clinically for kidney-targeted drug delivery.

Elastin-like Polypeptide (ELP) is a protein biopolymer composed of a repeating pentapeptide domain found in human elastin (51). ELP is advantageous as a drug carrier because its large size serves to stabilize small molecule drugs or peptide cargo from rapid clearance or degradation *in vivo* (5, 7, 37). Also, due to its roots as an elastin-based polypeptide, ELP is not recognized as foreign by the immune system (12, 41). Furthermore, in contrast to some synthetic polymer drug carriers, ELP can be slowly degraded into its natural amino acid building blocks, greatly limiting its potential to

induce unwanted adverse effects (28, 48). Since ELP is a genetically encoded protein, the core biopolymer can be modified by the addition of targeting or therapeutic peptides, proteins (6, 8, 18, 32, 36), or drug reactive sites (3, 11, 15, 27) by using simple molecular biology techniques to alter the ELP-encoding DNA.

We have previously used ELPs to deliver peptide and small molecule drug cargo in several disease models (4, 5, 17), and recently used direct intrarenal injection of an ELP-fused form of vascular endothelial growth factor (VEGF) to recover renal function and improve the kidney microvasculature in a clinically relevant swine model of chronic renovascular disease (10). Previous studies have demonstrated strong renal accumulation of ELP (4, 5), which is further increased when ELPs are modified with positively charged cell-penetrating peptides (CPPs) (4) that enhance the cellular uptake of macromolecules by mediating adherence to or passage across biological membranes (2). However, CPPs tend to have poor organ-targeting properties, increasing polypeptide deposition in most major organs (45).

To the best of our knowledge, no organ-specific targeting of ELP has been achieved using peptide-targeting agents. Here we describe a biodegradable, non-immunogenic protein-based biopolymer that is actively targeted to the kidney using a kidney-selective peptide targeting domain (43). We fused the coding sequence for this kidney targeting peptide (KTP), flanked by two cysteine residues to encourage cyclization, to the ELP coding sequence to generate a kidney-targeted version of the ELP carrier (KTP-ELP). Using rat and swine models, we assessed the *in vivo* pharmacokinetics, biodistribution, intrarenal localization, renal function and toxicity, *in vitro* renal cell type binding, and *in vitro* cytotoxicity of KTP-ELP, compared to the untargeted parent molecule ELP or to two previously-described CPP-modified ELPs, Tat-ELP (52, 31, 30) and SynB1-ELP (46, 8, 17).

Materials and Methods.

Expression Vector Construction, Polypeptide Purification, and Fluorescent Labeling. The coding sequence for ELP was modified by the addition of the coding sequence for KTP (LPVAS),

flanked by two cysteine residues to promote cyclization, at the N-terminus and by addition of a C-terminal cysteine residue for fluorophor conjugation. The expression constructs for ELP and the CPP-conjugated SynB1-ELP and Tat-ELP were from the lab of Drazen Raucher and published previously (31, 37). The makeup of the KTP and CPP-fused ELPs is shown in Figure 1. All proteins were purified by inverse transition cycling as described previously (6, 18). The polypeptides were labeled with maleimide conjugates of fluorescein, rhodamine, or AlexaFluor 633 (Life technologies) as described in (6) with one modification. When labeling KTP-ELP, no pre-labeling reducing step was carried out in order to label only the free C-terminal cysteine and not interfere with the cyclization of KTP.

***In vivo* Biodistribution Studies.** Animal studies were approved by the Animal Care and Use Committee of the University of Mississippi Medical Center and conducted according to the guidelines of the Guide for the Care and Use of Laboratory Animals (40). For acute tissue biodistribution studies, hairless Sprague Dawley rats (Charles River) were anesthetized with isoflurane (1 – 3%, to effect) and administered rhodmaine-labeled polypeptides (100 mg/kg) by intravenous injection into the femoral vein. Four hours after injections, rats were euthanized while still under anesthesia, and organs were collected for whole-organ fluorescence biodistribution analysis as described below (n = 4 rats per agent). For longer-term pharmacokinetic and whole-body fluorescence experiments, hairless Sprague Dawley rats (n = 3 rats per agent) were injected with ELP or KTP-ELP intravenously (100 mg/kg, femoral vein), and blood was sampled intermittently after injection by nicking the tail vein. Whole-animal fluorescence images were collected at regular intervals for 24 hours using an IVIS Spectrum (Perkin Elmer).

For pharmacokinetic and biodistribution experiments in swine, domestic crossbred female pre-juvenile pigs (*sus scrofa domestica*) were anesthetized, and cannulas were placed in the ear vein for administration of test agents and in the carotid artery for blood sampling. Pigs were maintained under isoflurane anesthesia (1 – 3 %, to effect) for the entire study with continuous monitoring of heart and

respiratory rate and oxygen saturation. ELP, KTP-ELP (5 mg/kg reconstituted in saline + 50 μg/mL polymixin B), or saline control was administered via the ear vein in a total volume of 10 mL (n = 3 pigs per agent). Blood was collected immediately before injection and at the indicated time points after protein administration. Plasma was separated by centrifugation for fluorescence analysis as described below. Four hours after injection, the pig was euthanized by an overdose of intravenous pentobarbital (100 mg/kg), and organs were immediately harvested for *ex vivo* fluorescence analysis.

Organ biodistribution in both rats and pigs was determined by *ex vivo* imaging of all major organs four hours after injection using an IVIS Spectrum as described in (17). Pharmacokinetics were determined in rats and pigs by direct fluorescence measurement as described in (5). Percentage of plasma fluorescence resulting from free fluorophor was determined by precipitating all proteins by mixing plasma 1:1 with 10% tricholoracetic acid, centrifugation, and re-analysis of fluorescence.

Whole-body fluorescence was measured in rats by collecting dorsal and ventral view images of the live animal at various time points after polypeptide injection using an IVIS Spectrum. Images were collected using 535 nm excitation and 580 nm emission filters, auto exposure, and small binning. Regions of interest (ROIs) were drawn over the entire animal, and mean radiant efficiency was measured to determine whole-body fluorescence intensity. Standard curves of each injected protein were pipetted into a black 96-well plate, which was subsequently imaged with identical imaging parameters. Mean tissue fluorescence was fit to these standard curves to correct for any differences in labeling levels among polypeptides.

Immunohistochemistry. Rat kidneys were flash frozen and cut into 20 μm sections with a cryomicrotome. Sections were fixed with 4% paraformaldehyde for 10 minutes at room temperature, then blocked 30 minutes with1% BSA and washed three times with PBS. Sections were incubated overnight at 4 °C with primary antibody (anti-CD31 Rabbit polyclonal, 1:300; anti-Synaptopodin Rabbit polyclonal, 1: 500; from Abcam), followed by incubation with secondary antibody (Alexa Fluor 488 goat anti-rabbit IgG, 1:400, Invitrogen) for 30 minutes at room temperature. Slides were washed

3 x 5 min, stained with DAPI for 1 min, washed with PBS for 2 min, dried, and coverslipped. Cortical samples of pig kidneys were flash frozen and cut into 14 μm sections with a cryomicrotome. Sections were fixed with 4% paraformaldehyde, stained with DAPI as above, and coverslipped. Images were collected by laser scanning confocal microscopy (Nikon C2+) using 405, 488, 561, and 640 nm lasers for excitation of DAPI, Alexa Fluor 488, rhodamine – labeled protein, and Alexa Fluor 633 – labeled protein, respectively. Five percent laser power and equal gain settings were used for all images.

Renal Function Assays. Female CD hairless rats, 6-8 weeks old, were acquired from Charles River Laboratories (Raleigh, NC) and used in FITC-sinistrin clearance assays. Standard rodent chow and water were administered *ad libitum*, and body weights were recorded daily. When the rodents achieved an average body weight of ~ 200 grams, the rats were placed into three treatment groups (n = 8 rats / group): saline, ELP (10 mg/kg/day), and KTP-ELP (10 mg/kg/day). Alzet® 2ML2 osmotic pumps (Cupertino, CA), with a flow rate of 5 μL/hr, were aseptically prepared with either sterile DBPS (HyClone Laboratories, Logan, UT), ELP, or KTP-ELP at a dosage of 10 mg/kg/day. Under isoflurane anesthesia (3%), the rats were subcutaneously administered carprofen (5 mg/kg) for analgesia, and were placed in the supine position on a surgical heating pad set at 37°C. A midline incision was performed on the abdominal region, and an osmotic pump was implanted into the right side of the peritoneal cavity. The incision was closed with 3-0 sterile nylon non-absorbable sutures (S. Jackson, Inc., Alexandria, VA), and the animals were returned to home cages to recover. Post-surgical monitoring, acquisition of body weights, and administration of bacon-flavored rimadyl (2 mg/tablet) (Bio-Serv, Flemington, NJ) for analgesia were performed daily for 14 days.

Thirteen days following the intraperitoneal implantation of osmotic pumps, the rats were transferred to metabolic cages for urine collection. Rats were removed from their home cages and transferred to individual sterilized, stainless steel metabolic cages, each of which provided with 100 mL of water and unlimited standard rodent chow. Rats remained in the metabolic cages for 24 hours to collect urine for urinalysis as described below. After 24 hours in metabolic cage housing, the rats

were weighed, the amount of urine collected (mL), and the amount of water consumed (mL) were recorded.

Under light isoflurane anesthesia (1-3%), each animal was fitted on the skin between the scapulae with an optical split device (Mannheim Pharma and Diagnostics GmbH, Mannheim, Germany) that contained two LEDs that excited the FITC-sinistrin and a photodiode to detect the fluorescent signal (21). The optical split device with battery was secured to the animal with flexible, elastic wound dressing wrap (Johnson and Johnson, Neewah, WI) and double-sided adhesive tape. The rat was placed in the supine position, and a one-inch incision was made at 2-3 mm lateral to most caudal mammary glands to expose the left femoral vein. A bolus dose of 7.5 mg/100 g body weight FITC-Sinistrin (Fresenius Kabi GmbH, Austria) in 0.2 cm^3 sterile DPBS (Hyclone Laboratories, Logan, UT) was delivered via the left femoral vein with a 30-gauge needle. Sterile wound clips were applied to close the incision, and the rat was returned to its singly housed home cage. Data were collected, in units of mL/min per 100 g body weight, and GFR was calculated with the equation GFR = 31.26 [mL/100 g body weight] / $t_{1/2}$ (FITC-Sinistrin) [min] (13, 38, 44, 47). The factor of 31.26 [mL/100 g body weight] was acquired by multiplying the mean half-life ($t_{1/2}$) and mean GFR, which enables the calculation of GFR normalized per 100 g body weight (47). Both $t_{1/2}$ and GFR were calculated by employing a one-compartment model, where for the $t_{1/2}$, a single exponential regression was fitted through the data points of the concentration time curve between 30 and 120 minutes after femoral vein injection of FITC-Sinistrin (47).

Plasma and Urine Analysis. Following the 14-day dosing protocol, creatinine levels were assessed in both plasma and 24 hour urine samples using a commercial creatinine assay kit (BioAssay Systems, Hayward, CA). For the plasma samples, standards were diluted to 2 mg/dL as per the vendor recommendations, and 30 µL of standards and plasma were run in duplicate. Optical density was read immediately (OD_0), and then again at 5 minutes (OD_5) with a peak absorbance wavelength at 510 nm. To measure creatinine levels in the metabolic cage urine, the same commercial creatinine

kit was used, with a fresh 96-well plate, and standards diluted to 50 mg/dL. 5 µL of standards and metabolic cage urine samples were run in duplicate. OD_0 and OD_5 were read at 510 nm. For both the plasma and urine samples, creatinine concentration was calculated as $(OD_{sample5} – OD_{sample0})/(OD_{STD5} – OD_{STD0})$ x [STD] (mg/dL). $OD_{sample5}$, $OD_{sample0}$, OD_{STD5}, and OD_{STD0} are the OD_{510nm} values of sample and standard at 5 and 0 minutes, respectively.

Urine albumin levels were quantified with an albumin ELISA kit (Abcam, Cambridge, MA), where urine samples were diluted 1:200 with 1X diluent, and 50 µL of each diluted sample was applied per well. The absorbance of the diluted urine samples was read at 450 nm, with 750 nm as the reference wavelength. The data were fit with a four-parameter logistic curve using GraphPad Prism 6.

Renal Histology. Paraffin-embedded 5 µm renal mid-hilar cross-sections of each kidney (1 per animal) were stained with trichrome. Morphometric analysis was performed to assess renal fibrosis and glomerulosclerosis, as previously described (9, 22).

Cell Culture. Human Glomerular Microvascular Endothelial (HGME) cells were purchased from Cell Systems (Kirkland, WA) and subcultured according to manufacturer's recommendations using Attachment Factor™ and complete classic medium supplemented with Culture Boost™. Cells in passage 4-13 were used for all experiments. Human Renal Proximal Tubular Epithelial Cells (HRPTEpC) were purchased from Cell Applications, Inc. (San Diego, CA) and subcultured according to manufacturer's recommendations using RenaEpi Growth factor media. Cells in passage 2-4 were used for all experiments. Human Podocyte Cells were purchased from Celprogen (Torrance, CA) and subcultured according to manufacturer's recommendations using human Podocyte cell culture media plus serum. The cells were seeded in ECM coated flasks or Microtiter plates purchased from Celprogen, and cells in passage 9-13 were used for all experiments. All cells were maintained at 37°C humidified incubator at 5% CO_2.

Flow Cytometry. HGME, HRPTEpC, and human Podocyte cells were seeded at 300,000 cells / well in 6 well plates (ECM coated plates were used for human Podocyte cells). Twenty four hours after seeding, the cells were washed and treated with fluorescein-labeled ELP, SynB1-ELP, Tat-ELP, or KTP-ELP at final concentration of 10 μM and incubated at 37 °C overnight. At the end of the incubation, the cells were washed with DPBS twice, and 500 μl of Cellstripper buffer (Mediatech,Inc) was added in each well followed by addition of 1 mL of DPBS, and cells were collected by centrifugation at 400xg. The relative fluorescence intensity of the cells was measured using a Gallios Flow Cytometer (BD Biosciences), and data were corrected for differences in labeling efficiency among proteins. Data represent the mean ± s.e.m. of three independent experiments performed in duplicate.

Cell Proliferation. HGME, HRPTEpC, and human Podocyte cells were seeded at 10,000 cells / well in 96 well plates (ECM coated plates were used for human Podocyte cells). Twenty four hours after seeding, the cells were serum and growth factor starved for 2-3 hours before treatment. After starvation, the proteins (ELP, SynB1-ELP, Tat-ELP, and KTP-ELP) were added at 100 μl volume in complete media to final concentrations of 5, 10, 20, and 40 μM and incubated for an additional 72 hours. Viable cells were detected using the MTS cell proliferation assay (Promega). The data shown represent the mean ± s.e.m. of three independent experiments in quadruplicate.

Statistical Analysis. Differences among polypeptide levels within each organ and among kidney:organ ratios, differences between treatment groups in all renal function assays, and differences among polypeptide cell binding/uptake were compared using a one-way ANOVA and *post hoc* Tukey's multiple comparison test. Cell proliferation data were compared with a two-way ANOVA with a *post hoc* Tukey's multiple comparison test for factors of polypeptide treatment and concentration. Alpha < 0.05 was taken as a statistically significant difference among groups, and

multiple comparisons were made using 95% confidence intervals. All statistical analysis was performed using Graphpad Prism.

Results.

The Kidney Targeting Peptide Enhances Kidney Levels and Kidney Specificity of ELP in a Rodent Model. Previous acute biodistribution studies have revealed high kidney deposition of ELP within 3-4 hours after systemic injection, and CPPs have been repeatedly shown to increase deposition in many organs, most profoundly in the kidneys (4, 17). In order to determine whether KTP also increases ELP levels in the kidney, and to compare the kidney specificity of KTP to previously used CPPs, an acute biodistribution experiment was performed in a rat model.

Four hours after intravenous injection of fluorescently-labeled ELP, SynB1-ELP, Tat-ELP, or KTP-ELP (Figure 1), the rats were euthanized, and organs were removed to quantify the polypeptides' biodistribution. *Ex vivo* organ imaging revealed that all polypeptides accumulated most strongly in the kidney, the liver had the second highest polypeptide levels, and all other major organs had lower levels (Figure 2A and B). The addition of the SynB1 or Tat CPPs increased kidney levels approximately 4.2 and 3.6-fold, respectively, and increased uptake in the liver 2.8- and 2.2-fold, respectively, relative to untargeted ELP. KTP increased kidney levels 4.9-fold relative to ELP, but caused no significantly increased deposition in any other organ. In fact, KTP-ELP was present at reduced levels relative to SynB1-ELP in the heart and brain and was completely undetectable in the spleen (Figure 2B). The total kidney levels of KTP-ELP were significantly higher than Tat-ELP levels but not statistically different from SynB1-ELP levels.

To further assess organ specificity, ratios of kidney levels to other organ levels were calculated. As shown in Figure 2C, KTP accumulated in the kidney at levels 15-fold higher than in the liver, and this enhancement was significantly higher than the kidney:liver ratios for ELP, SynB1-ELP, or Tat-ELP. Similarly, KTP-ELP kidney levels were about 150-fold higher than heart levels, and

this ratio was significantly higher than any other polypeptide (Figure 2D). These data indicate that both CPPs and KTP mediate deposition of ELP in the kidney, but KTP has much higher specificity for the kidney than the CPPs.

The Kidney Targeting Peptide Extends Plasma Half-life and Tissue Residence Time in a Rodent Model. To determine the effects of KTP on the plasma pharmacokinetics and total tissue levels of ELP, an extended biodistribution experiment was conducted in hairless Sprague Dawley rats. In this study, *in vivo* imaging of the live animal was used to measure total body fluorescence (including intravascular and tissue polypeptide levels) over time after injection, and plasma was sampled at each time point to determine plasma pharmacokinetics.

As shown in Figure 3A, plasma clearance was biphasic and fit well to a two-compartment pharmacokinetic model (Table 1). KTP-ELP cleared more slowly from the plasma than did ELP. The half-life of KTP-ELP was nearly four hours, compared to just less than one hour for ELP. This resulted in a nearly five-fold increase in area under the plasma curve (Table 1). Interestingly, the decrease in plasma fluorescence during the first few hours after injection was accompanied by an increase in whole-body fluorescence, likely indicating extravasation of the polypeptides. KTP had profound effects on the whole-body fluorescence kinetics. Unmodified ELP peaked in the tissues 1 hour after injection, then began slowly clearing from the body. In contrast, KTP-ELP showed a higher peak whole-body fluorescence (even after correction for any differences in labeling efficiency), and the tissue levels didn't reach their peak until 3 to 4 hours after injection (Figure 3B). KTP-ELP levels remained higher than ELP even at 24 h after injection, and the overall area under the curve of tissue levels was increased nearly 2-fold by the addition of KTP to ELP (Figure 3B). Loss of the fluorophor from the protein was not a concern, as nearly all the fluorescence signal was precipitated by incubation in 10% trichloroacetic acid, indicating that the fluorophor remained protein bound (Figure 3C). These data indicate that the KTP peptide may enhance extravasation of ELP, thereby extending its plasma half-life and tissue residence time. While the plasma half-lives of these polypeptides are

on the order of hours, much of the loss in plasma is due to extravasation in tissues (mostly in the kidney), and the whole-body KTP-ELP levels remain significantly elevated for at least 24h after intravenous injection.

Intra-renal Distribution of Polypeptides. In addition to the whole-organ *ex vivo* imaging, fluorescence slide scanning of renal sections revealed that all polypeptides were mostly confined to the renal cortex (Figure 4A). Also, consistent with the whole-organ imaging, SynB1-ELP, Tat-ELP, and KTP-ELP accumulated to very high levels relative to the untargeted ELP biopolymer. When examined microscopically, KTP-ELP was localized in both the blood vessel walls (as indicated by CD31 staining, Figure 4B) and around the glomerulus (marked by synaptopodin staining, Figure 4C) in the surrounding tubules, but was not present in the interior of the glomerulus. A similar intrarenal distribution was seen for both ELP and KTP-ELP (Figure 4B and C). Specificity of the cell-type markers was confirmed by lack of signal in control slices stained without primary antibody (Figure 4D).

ELP and KTP-ELP Do Not Have Adverse Effects on Renal Function. Given the high kidney levels of the ELP and KTP-ELP biopolymers and the desire to use these proteins as kidney-targeted drug carriers in future applications, we sought to determine whether the proteins had adverse effects on renal function. To maximize the chances of finding any adverse effects, a chronic administration of a very high dose of ELP and KTP-ELP (10 mg/kg/day) was continuously administered to rats over 14 consecutive days. We first examined body weight as a general marker of polypeptide toxicity. As shown in Figure 5A, the continuous administration of ELP or KTP-ELP had no effect on body weight relative to saline control. The polypeptide treatment also had no effect on heart weight, kidney weight, water consumption, or urine output (Table 2).

At the end of the 14-day administration period, we determined glomerular filtration rate by measuring the clearance of FITC-sinistrin. As shown in Figure 5B, the polypeptides had no effect on

glomerular filtration rate. Urine albumin levels detected by ELISA demonstrated no significant differences between groups, further suggesting that KTP-ELP had no deleterious effect upon renal function. While urine creatinine levels (mg/dL) exhibited no differences among groups (Table 2), plasma creatinine levels in the KTP-ELP treated rats was slightly but statistically significantly elevated when compared to saline-treated rats. However, even in the KTP-ELP treated group, plasma creatinine levels remained well within the normal range previously reported by the Jaffe method in rats (42). Finally, the absence of deleterious effects on renal function was accompanied by a preserved renal parenchyma, as demonstrated by the morphometric analysis of tubule-interstitial and glomerular compartments showing a preserved renal parenchyma in ELP and KTP-ELP treated kidneys compared to saline-treated controls (Figure 5C).

Overall, these data strongly suggest that neither the ELP drug delivery carrier, nor the kidney targeting peptide interfere with renal function or induce renal damage.

KTP Effectively Targets ELP to the Kidneys in a Swine Model. To insure that the ability of KTP to target ELP to the kidneys was not specific to rats, a similar experiment was conducted in swine. As shown in Figure 6A, both ELP and KTP-ELP cleared from circulation with biphasic kinetics that fit well with a two-compartment pharmacokinetic model, consistent with the rodent data. There was no evidence of a significant amount of free dye present in the plasma at any time point (Figure 6B). KTP-ELP had a longer terminal plasma half-life and an increased area under the curve relative to ELP (Table 3). *Ex vivo* imaging revealed the significantly enhanced KTP-ELP levels in the kidney relative to ELP, and imaging the kidney in cross section revealed a mostly cortical distribution with some protien present in vascular structures (arrows, Figure 6C). KTP-ELP accumulated in the swine kidney at levels 5.4 fold higher than the untargeted ELP, and kidney KTP-ELP levels were 4.8-fold higher than liver, almost two-fold higher than lung, and over 50-fold higher than heart and spleen (Figure 6D).

Consistent with the intrarenal distribution of KTP-ELP in the rodent, confocal microscopy of cortical sections revealed a primarily tubular localization for KTP-ELP in the swine kindey (Figure 6E). KTP-ELP was present in the tubules at higher levels and with a more ubiqutous distribution than ELP. These data demonstrate that KTP is effective for kidney targeting in a translational preclinical model and is not species specific.

***In vitro* Cell-type Binding and Cytotoxicity of Polypeptides.** We sought to determine if KTP could enhance ELP binding to primary human renal cells and to identify for which cell type KTP has affinity. Primary human glomerular microvascular endothelial cells (HGME), primary human podocytes, and primary human renal proximal tubule epithelial cells (HRPTEpC) were exposed to 10 μM fluorescently labeled ELP, KTP-ELP, or CPP-ELP comparators. As shown in Figure 7A - C, KTP enhanced ELP binding to all renal cell types. Binding was increased 3 fold in HGME, 1.7 fold in podocytes, and 3 fold in HRPTEpC by KTP-ELP relative to ELP control. This was in contrast to the CPP-fused ELPs. Tat only enhanced ELP binding to HRPTEpC and actually reduced binding to podocytes. SynB1 only enhanced ELP binding to HGME cells and also reduced binding to podocytes. We also tested whether KTP-ELP had any toxicity to the human cell lines. Each cell line was incubated with polypeptides at concentrations up to 40 μM for 72 h. ELP, KTP-ELP, and SynB1-ELP showed no toxicity to any cell line tested (Figure 7D - F). In contrast, Tat-ELP was toxic to HGME cells. This is consistent with previous findings that Tat-ELP exhibits cell line dependent cytotoxicity in several cell types (19, 33).

These data demonstrate that KTP has affinity for several renal cell lines, and, in contrast to CPPs, it increases ELP binding to all renal cell types tested. These data also add to the swine data to insure that KTP is effective in rat, pig, and potentially human.

Discussion.

Our study characterizes a unique polypeptide drug carrier that combines passive renal targeting using a macromolecular carrier with active targeting using a kidney-specific peptide to achieve very high renal specificity. The kidney targeting peptide was originally discovered using a phage display technique (43), where it led to kidney accumulation in the mouse at levels 7 fold higher than in a comparator organ, the brain. Notably, our study shows that this peptide is capable of directing protein therapeutics to the kidney, and it does so in both rat and a translational swine model. Furthermore, *in vitro* experiments showed that KTP enhanced ELP binding to human renal cells with no observable cytotoxicity, and ELP or KTP-ELP had no adverse effects on renal function and induced no renal parenchymal damage even when administered at a very high dose. Therefore, the current study sets a translational stage for future development and application of a novel therapeutic tool for treatment of renal disease.

The intrarenal distribution of KTP-ELP was mostly tubular, with some additional polypeptide detected in vascular endothelial and underlying smooth muscle cells. The distribution along with the renal cell binding data raise questions regarding the mechanism of renal targeting by KTP. We observed a co-localization between KTP-ELP and endothelial cell markers that supports the possibility of KTP binding a vascular receptor and concurred with previous studies suggesting that the peptide may bind to a specifically expressed receptor in the renal vasculature (43). However, the phage-displayed peptide used in previous studies (43) was likely too large to be filtered by the glomerulus or to move out to the extra vascular space, which possibly played a role in limiting its distribution to the vascular endothelium. KTP-ELP has a molecular weight very near the renal filtration barrier (62 kDa), but the protein is uncharged and likely presents as an extended rod-like protein in solution (26), supporting a possibility of KTP-ELP being filtered by the glomerulus and reaching the tubules by protein reuptake. Interestingly, our study also detected KTP-ELP in tubular epithelial cells of the renal cortex, which could possibly be explained by the molecular weight of the construct. As little to no KTP-ELP signal was present within the glomerulus, it is also possible to

speculate that, alternatively, KTP-ELP may extravasate from peritubular capillaries and reach the tubular epithelium via a retrograde transport.

Based on the feasibility for modification to add drug reactive sites or genetically fused proteinaceous agents, KTP-ELP based treatments could be used as a strategy to deliver small molecule, protein, or peptide therapeutics for a variety of renal disorders. Given the presence of a free C-terminal thiol, KTP-ELP could easily be modified with a thiolated drug (such as captopril) in order to achieve kidney-specific delivery, or KTP-ELP could be used to deliver other small molecule drugs engineered with thiol reactive cleavable linkers. We are also currently developing ELP-fused growth factors for recovery of renal function by protecting the renal microcirculation in experimental CKD (10) or acute kidney injury. We recently reported the therapeutic efficacy of direct intrarenal injection of an ELP-fused form of VEGF to improve renal function and microvascular density in a swine model of chronic renal vascular disease (18). Microvascular disease is a hallmark of chronic renal disease from different etiologies and plays a central role in developing renal fibrosis (53), and the use of KTP-ELP technology could expand this application (18) by allowing a systemic but targeted strategy to protect the kidney. Another possibility we are exploring is the application of ELP technology for development of renal targeted anti-inflammatory strategies, since progressive renal inflammation is observed in CKD and suggested as a precursor of renal fibrosis (34, 49). Alternatively, KTP-ELPs could also be labeled with tracers for imaging studies or potentially as markers of renal function, underscoring the plasticity and potential of ELP-based technology for therapeutic and diagnostic applications.

However, we believe these promising findings are not free of questions that may need to be addressed by complementary studies in the near future. For example, the role of molecular weight on renal deposition and intrarenal distribution of KTP-ELP will be determined by modifying (e.g.: increasing or decreasing) the ELP polypeptide sequence to modulate the overall molecular weight of the carrier. Such studies might in turn identify a more optimal size of the ELP that will increase the feasibility of the carrier as a drug-delivery vector for renal targeting. On another note, although our

data show that KTP increases association of ELP with several renal cell types, we will further determine whether KTP binds a specific cellular receptor and/or serves as a cell penetrating peptide in its own right by crosslinking and protein sequencing studies to disclose any specific binding partner for the KTP peptide.

In summary, our study supports the potential for renal therapy of a novel and customizable drug delivery vector. Given KTP-ELP's efficient kidney targeting, low immunogenicity, low cytotoxicity, amenability for therapeutic attachment, and lack of species specificity, we believe our study lays the foundation for future development of kidney targeted ELPs as a platform for drug delivery for renal disease.

Acknowledgements. The authors would like to thank Rowshan Begum for assistance with polypeptide purification, Mariper Lopez for assistance with histology, and Drazen Raucher for providing the CPP-ELP expression vectors. CR was supported by the Summer Undergraduate Research Experience (SURE) program of the University of Mississippi Medical Center. Access to animal imaging equipment was provided by the Animal Imaging Core Facility at the University of Mississippi Medical Center. Flow cytometry was performed by the Flow Cytometry Core Facility at the University of Mississippi Medical Center.

Grants. This work was supported by NIH grant R01HL121527 to GLB and by NIH grant R01HL095638 and AHA grant 18490005 to ARC.

Disclosures. GLB is owner of Leflore Technologies, LLC, a private company working to translate ELP drug delivery technology. Leflore Technologies provided no funding for this work. GLB and ARC are authors of patents related to the renal targeting drug delivery technology.

References.

1. **American Kidney Fund**. Kidney Disease Statistics. 2015.

2. **van den Berg A**, **Dowdy SF**. Protein transduction domain delivery of therapeutic macromolecules. *Curr Opin Biotechnol* 22: 888–93, 2011.

3. **Bidwell GL**, **Fokt I**, **Priebe W**, **Raucher D**. Development of elastin-like polypeptide for thermally targeted delivery of doxorubicin. *Biochem Pharmacol* 73: 620–31, 2007.

4. **Bidwell GL**, **Perkins E**, **Hughes J**, **Khan M**, **James JR**, **Raucher D**. Thermally targeted delivery of a c-Myc inhibitory polypeptide inhibits tumor progression and extends survival in a rat glioma model. *PLoS One* 8: e55104, 2013.

5. **Bidwell GL**, **Perkins E**, **Raucher D**. A thermally targeted c-Myc inhibitory polypeptide inhibits breast tumor growth. *Cancer Lett* 319: 136–43, 2012.

6. **Bidwell GL**, **Raucher D**. Application of thermally responsive polypeptides directed against c-Myc transcriptional function for cancer therapy. *Mol Cancer Ther* 4: 1076–85, 2005.

7. **Bidwell GL**, **Raucher D**. Cell penetrating elastin-like polypeptides for therapeutic peptide delivery. *Adv Drug Deliv Rev* 62: 1486–96, 2010.

8. **Bidwell GL**, **Whittom AA**, **Thomas E**, **Lyons D**, **Hebert MD**, **Raucher D**. A thermally targeted peptide inhibitor of symmetrical dimethylation inhibits cancer-cell proliferation. *Peptides* 31: 834–41, 2010.

9. **Chade AR**, **Rodriguez-Porcel M**, **Grande JP**, **Krier JD**, **Lerman A**, **Romero JC**, **Napoli C**, **Lerman LO**. Distinct renal injury in early atherosclerosis and renovascular disease. *Circulation* 106: 1165–1171, 2002.

10. **Chade AR**, **Tullos NA**, **Harvey TW**, **Mahdi F**, **Bidwell GL**. Renal Therapeutic Angiogenesis Using a Bioengineered Polymer-Stabilized Vascular Endothelial Growth Factor Construct. *J. Am. Soc. Nephrol. JASN* (November 5, 2015). doi: 10.1681/ASN.2015040346.

11. **Chilkoti A**, **Dreher MR**, **Meyer DE**. Design of thermally responsive, recombinant polypeptide carriers for targeted drug delivery. *Adv Drug Deliv Rev* 54: 1093–111, 2002.

12. **Cho S**, **Dong S**, **Parent KN**, **Chen M**. Immune-tolerant elastin-like polypeptides (iTEPs) and their application as CTL vaccine carriers. *J Drug Target* 24: 328–339, 2016.

13. **Cowley AW**, **Ryan RP**, **Kurth T**, **Skelton MM**, **Schock-Kusch D**, **Gretz N**. Progression of glomerular filtration rate reduction determined in conscious Dahl salt-sensitive hypertensive rats. *Hypertens Dallas Tex 1979* 62: 85–90, 2013.

14. **Franssen EJ**, **van Amsterdam RG**, **Visser J**, **Moolenaar F**, **de Zeeuw D**, **Meijer DK**. Low molecular weight proteins as carriers for renal drug targeting: naproxen-lysozyme. *Pharm Res* 8: 1223–1230, 1991.

15. **Furgeson DY**, **Dreher MR**, **Chilkoti A**. Structural optimization of a “smart” doxorubicin-polypeptide conjugate for thermally targeted delivery to solid tumors. *J Control Release* 110: 362–9, 2006.

16. **Geng Q**, **Sun X**, **Gong T**, **Zhang Z-R**. Peptide-drug conjugate linked via a disulfide bond for kidney targeted drug delivery. *Bioconjug Chem* 23: 1200–1210, 2012.

17. **George EM**, **Liu H**, **Robinson GG**, **Bidwell GL**. A polypeptide drug carrier for maternal delivery and prevention of fetal exposure. *J. Drug Target.* (August 22, 2014). doi: 10.3109/1061186X.2014.950666.

18. **George EM**, **Liu H**, **Robinson GG**, **Mahdi F**, **Perkins E**, **Bidwell GL**. Growth factor purification and delivery systems (PADS) for therapeutic angiogenesis. *Vasc Cell* 7: 1, 2015.

19. **George EM**, **Mahdi F**, **Logue OC**, **Robinson GG**, **Bidwell GL**. Corneal Penetrating Elastin-Like Polypeptide Carriers. *J. Ocul. Pharmacol. Ther. Off. J. Assoc. Ocul. Pharmacol. Ther.* (December 16, 2015). doi: 10.1089/jop.2015.0082.

20. **Haas M**, **Kluppel AC**, **Wartna ES**, **Moolenaar F**, **Meijer DK**, **de Jong PE**, **de Zeeuw D**. Drug-targeting to the kidney: renal delivery and degradation of a naproxen-lysozyme conjugate in vivo. *Kidney Int* 52: 1693–1699, 1997.

21. **Herrera Pérez Z**, **Weinfurter S**, **Gretz N**. Transcutaneous Assessment of Renal Function in Conscious Rodents. *J Vis Exp JoVE* : e53767, 2016.

22. **Iliescu R**, **Chade AR**. Progressive renal vascular proliferation and injury in obese Zucker rats. *Microcirc N Y N 1994* 17: 250–258, 2010.

23. **Kok RJ**, **Grijpstra F**, **Walthuis RB**, **Moolenaar F**, **de Zeeuw D**, **Meijer DK**. Specific delivery of captopril to the kidney with the prodrug captopril-lysozyme. *J Pharmacol Exp Ther* 288: 281–285, 1999.

24. **L'azou B**, **Jorly J**, **On D**, **Sellier E**, **Moisan F**, **Fleury-Feith J**, **Cambar J**, **Brochard P**, **Ohayon-Courtès C**. In vitro effects of nanoparticles on renal cells. *Part Fibre Toxicol* 5: 22, 2008.

25. **Lin Y**, **Li Y**, **Wang X**, **Gong T**, **Zhang L**, **Sun X**. Targeted drug delivery to renal proximal tubule epithelial cells mediated by 2-glucosamine. *J Control Release Off J Control Release Soc* 167: 148–156, 2013.

26. **Lyons DF**, **Le V**, **Bidwell GL 3rd**, **Kramer WH**, **Lewis EA**, **Raucher D**, **Correia JJ**. Structural and hydrodynamic analysis of a novel drug delivery vector: ELP[V5G3A2-150]. *Biophys J* 104: 2009–2021, 2013.

27. **MacKay JA**, **Chen M**, **McDaniel JR**, **Liu W**, **Simnick AJ**, **Chilkoti A**. Self-assembling chimeric polypeptide-doxorubicin conjugate nanoparticles that abolish tumours after a single injection. *Nat Mater* 8: 993–9, 2009.

28. **Mackay JA**, **Chilkoti A**. Temperature sensitive peptides: engineering hyperthermia-directed therapeutics. *Int J Hyperth Off J Eur Soc Hyperthermic Oncol North Am Hyperth Group* 24: 483–495, 2008.

29. **Manil L**, **Davin JC**, **Duchenne C**, **Kubiak C**, **Foidart J**, **Couvreur P**, **Mahieu P**. Uptake of nanoparticles by rat glomerular mesangial cells in vivo and in vitro. *Pharm Res* 11: 1160–1165, 1994.

30. **Massodi I**, **Bidwell GL**, **Davis A**, **Tausend A**, **Credit K**, **Flessner M**, **Raucher D**. Inhibition of ovarian cancer cell metastasis by a fusion polypeptide Tat-ELP. *Clin Exp Metastasis* 26: 251–60, 2009.

31. **Massodi I**, **Bidwell GL**, **Raucher D**. Evaluation of cell penetrating peptides fused to elastin-like polypeptide for drug delivery. *J Control Release* 108: 396–408, 2005.

32. **Massodi I**, **Moktan S**, **Rawat A**, **Bidwell GL**, **Raucher D**. Inhibition of ovarian cancer cell proliferation by a cell cycle inhibitory peptide fused to a thermally responsive polypeptide carrier. *Int J Cancer* 126: 533–44, 2010.

33. **Massodi I**, **Raucher D**. A thermally responsive Tat-elastin-like polypeptide fusion protein induces membrane leakage, apoptosis, and cell death in human breast cancer cells. *J Drug Target* 15: 611–22, 2007.

34. **Meng X-M**, **Nikolic-Paterson DJ**, **Lan HY**. Inflammatory processes in renal fibrosis. *Nat Rev Nephrol* 10: 493–503, 2014.

35. **Milić M**, **Leitinger G**, **Pavičić I**, **Zebić Avdičević M**, **Dobrović S**, **Goessler W**, **Vinković Vrček I**. Cellular uptake and toxicity effects of silver nanoparticles in mammalian kidney cells. *J Appl Toxicol JAT* 35: 581–592, 2015.

36. **Moktan S**, **Raucher D**. Anticancer activity of proapoptotic peptides is highly improved by thermal targeting using elastin-like polypeptides. *Int J Pept Res Ther* 18: 227–237, 2012.

37. **Moktan S**, **Ryppa C**, **Kratz F**, **Raucher D**. A thermally responsive biopolymer conjugated to an acid-sensitive derivative of paclitaxel stabilizes microtubules, arrests cell cycle, and induces apoptosis. *Invest New Drugs* (October 12, 2010). doi: 10.1007/s10637-010-9560-x.

38. **Mori T**, **Polichnowski A**, **Glocka P**, **Kaldunski M**, **Ohsaki Y**, **Liang M**, **Cowley AW**. High perfusion pressure accelerates renal injury in salt-sensitive hypertension. *J Am Soc Nephrol JASN* 19: 1472–1482, 2008.

39. **National Kidney and Urologic Diseases Information Clearinghouse; National Institute of Diabetes and Digestive and Kidney Diseases; National Institutes of Health**. Kidney Disease Statistics for the United States. 2012.

40. **National Research Council (US) Committee for the Update of the Guide for the Care and Use of Laboratory Animals**. *Guide for the Care and Use of Laboratory Animals*. 8th ed. Washington (DC): National Academies Press (US), 2011.

41. **Nouri FS**, **Wang X**, **Chen X**, **Hatefi A**. Reducing the Visibility of the Vector/DNA Nanocomplexes to the Immune System by Elastin-Like Peptides. *Pharm Res* 32: 3018–3028, 2015.

42. **Palm M**, **Lundblad A**. Creatinine concentration in plasma from dog, rat, and mouse: a comparison of 3 different methods. *Vet Clin Pathol Am Soc Vet Clin Pathol* 34: 232–236, 2005.

43. **Pasqualini R**, **Ruoslahti E**. Organ targeting in vivo using phage display peptide libraries. *Nature* 380: 364–6, 1996.

44. **Pill J**, **Kraenzlin B**, **Jander J**, **Sattelkau T**, **Sadick M**, **Kloetzer H-M**, **Deus C**, **Kraemer U**, **Gretz N**. Fluorescein-labeled sinistrin as marker of glomerular filtration rate. *Eur J Med Chem* 40: 1056–1061, 2005.

45. **Reissmann S**. Cell penetration: scope and limitations by the application of cell-penetrating peptides. *J Pept Sci Off Publ Eur Pept Soc* 20: 760–784, 2014.

46. **Rousselle C**, **Clair P**, **Lefauconnier JM**, **Kaczorek M**, **Scherrmann JM**, **Temsamani J**. New advances in the transport of doxorubicin through the blood-brain barrier by a peptide vector-mediated strategy. *Mol Pharmacol* 57: 679–86, 2000.

47. **Schock-Kusch D**, **Sadick M**, **Henninger N**, **Kraenzlin B**, **Claus G**, **Kloetzer H-M**, **Weiss C**, **Pill J**, **Gretz N**. Transcutaneous measurement of glomerular filtration rate using FITC-sinistrin in rats. *Nephrol Dial Transplant Off Publ Eur Dial Transpl Assoc - Eur Ren Assoc* 24: 2997–3001, 2009.

48. **Shah M**, **Hsueh P-Y**, **Sun G**, **Chang HY**, **Janib SM**, **MacKay JA**. Biodegradation of elastin-like polypeptide nanoparticles. *Protein Sci Publ Protein Soc* 21: 743–750, 2012.

49. **Shankar A**, **Sun L**, **Klein BEK**, **Lee KE**, **Muntner P**, **Nieto FJ**, **Tsai MY**, **Cruickshanks KJ**, **Schubert CR**, **Brazy PC**, **Coresh J**, **Klein R**. Markers of inflammation predict the long-term risk of developing chronic kidney disease: a population-based cohort study. *Kidney Int* 80: 1231–1238, 2011.

50. **Suzuki K**, **Susaki H**, **Okuno S**, **Sugiyama Y**. Renal drug targeting using a vector “alkylglycoside.” *J Pharmacol Exp Ther* 288: 57–64, 1999.

51. **Urry DW**, **Long MM**, **Cox BA**, **Ohnishi T**, **Mitchell LW**, **Jacobs M**. The synthetic polypentapeptide of elastin coacervates and forms filamentous aggregates. *Biochim Biophys Acta* 371: 597–602, 1974.

52. **Vives E**, **Brodin P**, **Lebleu B**. A truncated HIV-1 Tat protein basic domain rapidly translocates through the plasma membrane and accumulates in the cell nucleus. *J Biol Chem* 272: 16010–7, 1997.

53. **Xavier S**, **Vasko R**, **Matsumoto K**, **Zullo JA**, **Chen R**, **Maizel J**, **Chander PN**, **Goligorsky MS**. Curtailing endothelial TGF-β signaling is sufficient to reduce endothelial-mesenchymal transition and fibrosis in CKD. *J Am Soc Nephrol JASN* 26: 817–829, 2015.

54. **Yuan Z-X**, **Sun X**, **Gong T**, **Ding H**, **Fu Y**, **Zhang Z-R**. Randomly 50% N-acetylated low molecular weight chitosan as a novel renal targeting carrier. *J Drug Target* 15: 269–278, 2007.

55. **Zhou P**, **Sun X**, **Zhang Z**. Kidney-targeted drug delivery systems. *Acta Pharm Sin B* 4: 37–42, 2014.

56. **Zou J**, **Glinsky VV**, **Landon LA**, **Matthews L**, **Deutscher SL**. Peptides specific to the galectin-3 carbohydrate recognition domain inhibit metastasis-associated cancer cell adhesion. *Carcinogenesis* 26: 309–318, 2005.

57. **Zuckerman JE**, **Davis ME**. Targeting therapeutics to the glomerulus with nanoparticles. *Adv Chronic Kidney Dis* 20: 500–507, 2013.

Figure Legends.

Figure 1. Overview of Polypeptides used in this Study. The sequence of the targeting agents and overview of the ELP structure for all polypeptides used in this study is shown.

Figure 2. Enhancement of Kidney Specificity using Kidney Targeting Peptides. Rats were administered fluorescently labeled ELP, SynB1-ELP, Tat-ELP, or KTP-ELP, and organ biodistribution was determined by *ex vivo* fluorescence imaging (**A.**). Quantitative analysis showed that the highest accumulation of all peptides was in the kidney (**B.**), and the targeting agents significantly increased kidney specificity as assessed by kidney:liver and kidney:heart ratios (**C.** and **D.**).

*,# Statistically significant difference between indicated groups as assessed by a one-way ANOVA with post hoc Tukey's multiple comparison.

**, Polypeptide levels undetectable over autofluorescence.

Figure 3. Plasma and Tissue Pharmacokinetics of KTP-ELP and ELP. Blood was sampled and whole-body *in vivo* images were collected at various time points up to 24 h after bolus intravenous injection. Plasma data were fit to a two compartment pharmacokinetic model (**A.**). *In vivo* images were quantified to determine the mean fluorescence radiant efficiency at each time point to elucidate peak tissue levels and whole-body clearance kinetics (**B.**). Effects of fluorophor loss from polypeptides were assessed by measuring the plasma fluorescence before and after precipitation of the proteins with trichloroacetic acid (TCA). Fluorescence levels after TCA were corrected for dilution and compared to the pre-precipitation fluorescence to calculate the percentage of free dye at each time point (**C.**).

Figure 4. Intrarenal Distribution of Renally Targeted ELPs: Four hours after intravenous infusion of fluorescently labeled ELP, SynB1-ELP, Tat-ELP, or KTP-ELP, rat kidneys were rapidly frozen and

cut into 20 μm sections. **A.** Slides were scanned using a fluorescence slide scanner. Identical scan settings were used in order to directly compare the total kidney levels. **B and C.** Slides were stained with CD31 to mark blood vessels (green, **B.**) or synaptopodin to mark podocytes (green, **C.**), and KTP-ELP-rhodamine (red) was imaged using confocal microscopy (scale bar = 50 μm). Specificity of antibody cell type markers was confirmed by lack of signal when the primary antibody was omitted from the staining protocol (**D.**).

Figure 5. Chronic infusion of ELP and KTP-ELP do not have adverse effects on kidney function or development of renal injury. During a 14-day infusion of saline, ELP, or KTP-ELP (10 mg/kg/day), daily body weights were recorded (**A.**). On the final day of infusion, renal function was measured by the FITC-sinistrin clearance method (**B.**). Bars represent the mean ± s.d. of 8 rats per group, with individual animals' values shown by the markers. (**C.**) Representative renal cross-section (trichrome, 40x) showing the absence of renal fibrosis and preserved renal parenchyma in ELP and KTP-ELP treated kidneys compared to saline-treated controls.

Figure 6. KTP enhances ELP deposition in the swine kidney after IV administration. Pigs were given fluorescently labeled ELP or KTP-ELP by intravenous injection. Plasma was sampled intermittently for determination of polypeptide clearance (**A.**), and plasma clearance data were fit using a two compartment pharmacokinetic model. The presence of unbound dye in the plasma at each time point was assessed by TCA precipitation and fluorescence measurement (**B.**). Kidney distribution was determined 4 h after injection by *ex vivo* whole organ fluorescence imaging in both intact and vertically sliced kidneys (**C.**, arrows indicated major vascular areas). Whole organ *ex vivo* fluorescence of kidneys and other major organs were quantified relative to standard curves of each agent (**D.**). Intra-renal distribution was determined by confocal microscopy (**E.**) (scale bar = 100 μm).

Figure 7. KTP-ELP enhances ELP binding to human renal cells. Cell binding (**A.-C.**) and cell survival (**D.-F.**) of SynB1-ELP, Tat-ELP, and KTP-ELP relative to ELP control were determined by flow cytometry and a cell viability assay, respectively, in primary human glomerular microvascular endothelial cells (**A.,D.**), primary human podocytes (**B.,E.**), and primary human proximal tubule epithelial cells (**C.,F.**).

Table 1. Pharmacokinetics of ELP and KTP-ELP in Rodents.

			ELP	KTP-ELP
Central Compartment Volume of Distribution	V_c	(mL)	16.4	7.3
Plasma Clearance	*Cl*	(mL·min^{-1})	0.43	0.04
Area Under Curve	*AUC*	(μg·min·mL^{-1})	68,907.6	350,657.1
Distribution Half Life	$t_{1/2,dist}$	(min)	3.63	39.12
Terminal Half Life	$t_{1/2,term}$	(min)	52.6	234.83

Table 2. General Characteristics of Rats Exposed to 14 day Continuous Infusion of Test Agents.

		Saline	ELP	KTP-ELP	ANOVA p value
Water Consumption	mL / 24 h	25.50 ± 8.16	39.25 ± 20.98	29.50 ± 9.71	0.16
Urine Production	mL / 24 h	12.88 ± 3.04	15.56 ± 6.68	13.50 ± 1.69	0.45
Plasma Creatinine	mg / dL	0.29 ± 0.03	0.30 ± 0.03	0.34 ± 0.03 †	0.01 *
Urine Creatinine	mg / dL	35.82 ± 6.52	29.92 ± 13.51	38.36 ± 10.05	0.27
Albuminuria	µg / mL	9.53 ± 4.98	10.56 ± 5.59	11.81 ± 3.94	0.65
Heart Weight	g	0.93 ± 0.06	0.94 ± 0.11	1.06 ± 0.11	0.16
Kidney Weight	g	1.14 ± 0.07	1.07 ± 0.10	1.08 ± 0.06	0.18

* Statistically significant by one-way ANOVA ($p < 0.05$). † Statistically different from saline group, post hoc Tukey's multiple comparison

663 **Table 3. Pharmacokinetics of ELP and KTP-ELP in Swine.**
664

			ELP	KTP-ELP
Central Compartment Volume of Distribution	V_c	(mL)	1,316.9	1,214.5
Plasma Clearance	*Cl*	(mL·min^{-1})	24.3	15.3
Area Under Curve	*AUC*	(μg·min·mL^{-1})	5,962.3	9,472.7
Distribution Half Life	$t_{1/2,dist}$	(min)	3.8	6.0
Terminal Half Life	$t_{1/2,term}$	(min)	90.3	118.6

665

Figure 1. (New)

Polypeptide	Sequence
ELP	MCGPGVG $(VPGxG)_{160}$ VPGWPGSG *
SynB1-ELP	MRGGRLSYSRRRFSTSTGRGPGVG $(VPGxG)_{160}$ VPGWPGSGGC
Tat-ELP	MYGRKKRRQRRRGGPGVG $(VPGxG)_{160}$ VPGWPGSGGC
KTP-ELP	MCLPVASCGGPGVG $(VPGxG)_{160}$ VPGWPGSGGC

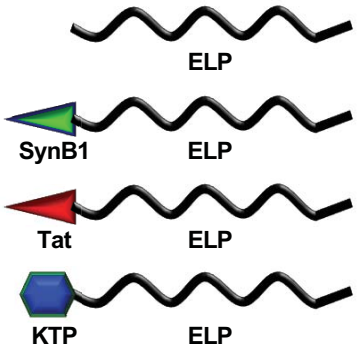

* x = Val, Gly, or Ala in a 1:7:8 ratio

Figure 2.

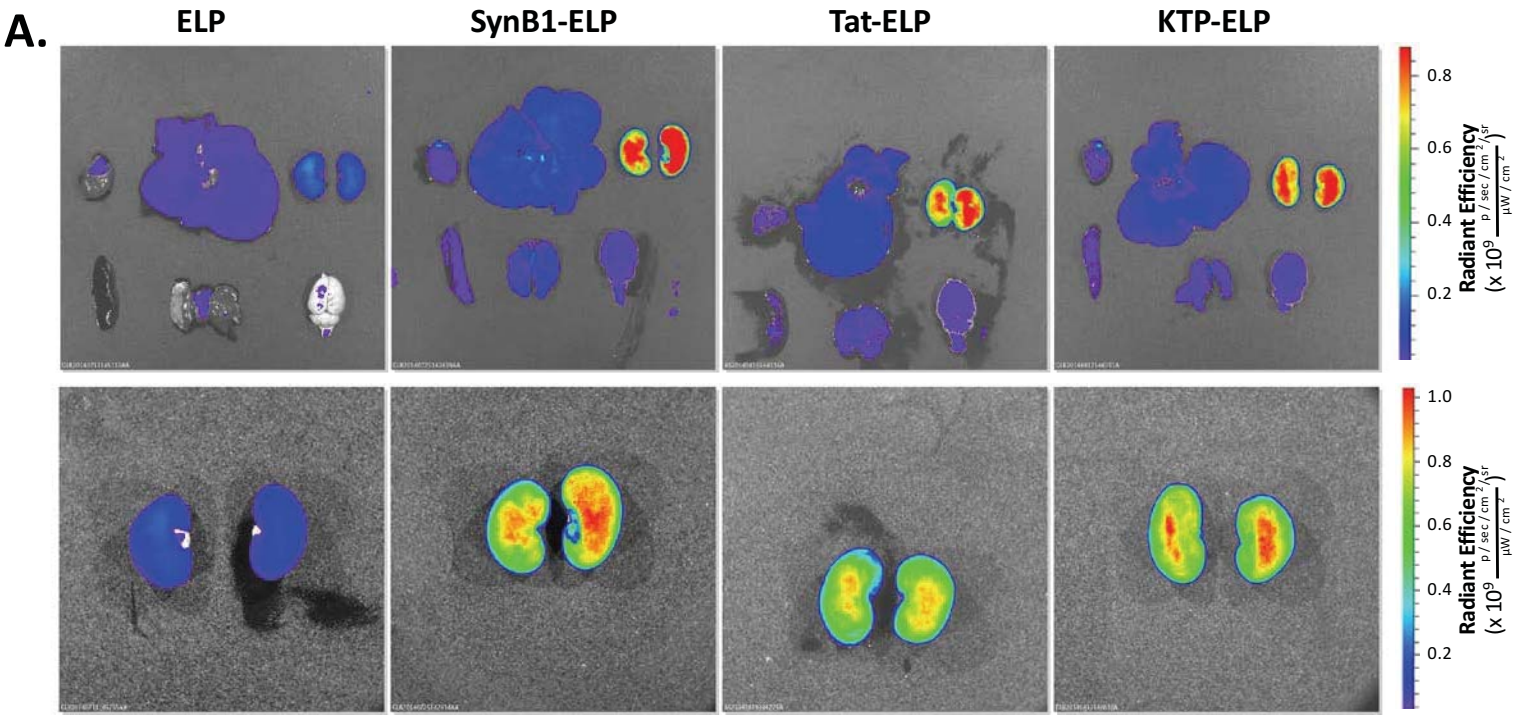
A.
ELP
SynB1-ELP
Tat-ELP
KTP-ELP
Radiant Efficiency
(x 10^9 p / sec / cm^2 / sr / µW / cm^2)
0.8
0.6
0.4
0.2
1.0

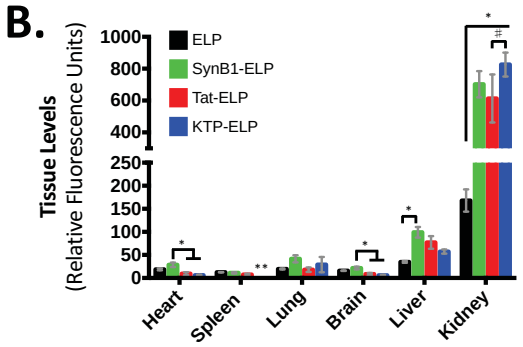
B.
Tissue Levels
(Relative Fluorescence Units)
ELP
SynB1-ELP
Tat-ELP
KTP-ELP
Heart
Spleen
Lung
Brain
Liver
Kidney

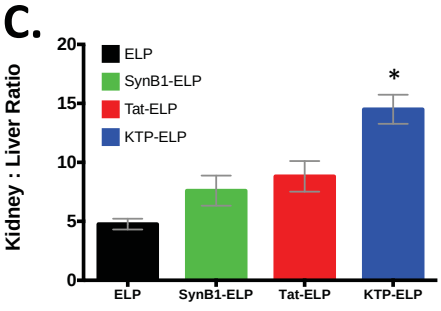
C.
Kidney : Liver Ratio
ELP
SynB1-ELP
Tat-ELP
KTP-ELP

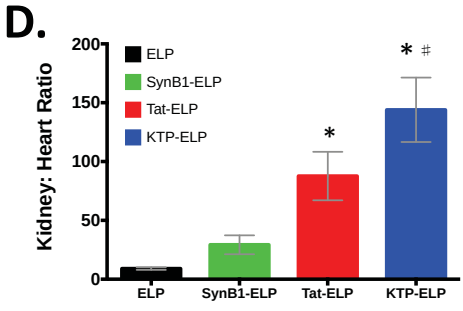
D.
Kidney: Heart Ratio
ELP
SynB1-ELP
Tat-ELP
KTP-ELP

Figure 3.

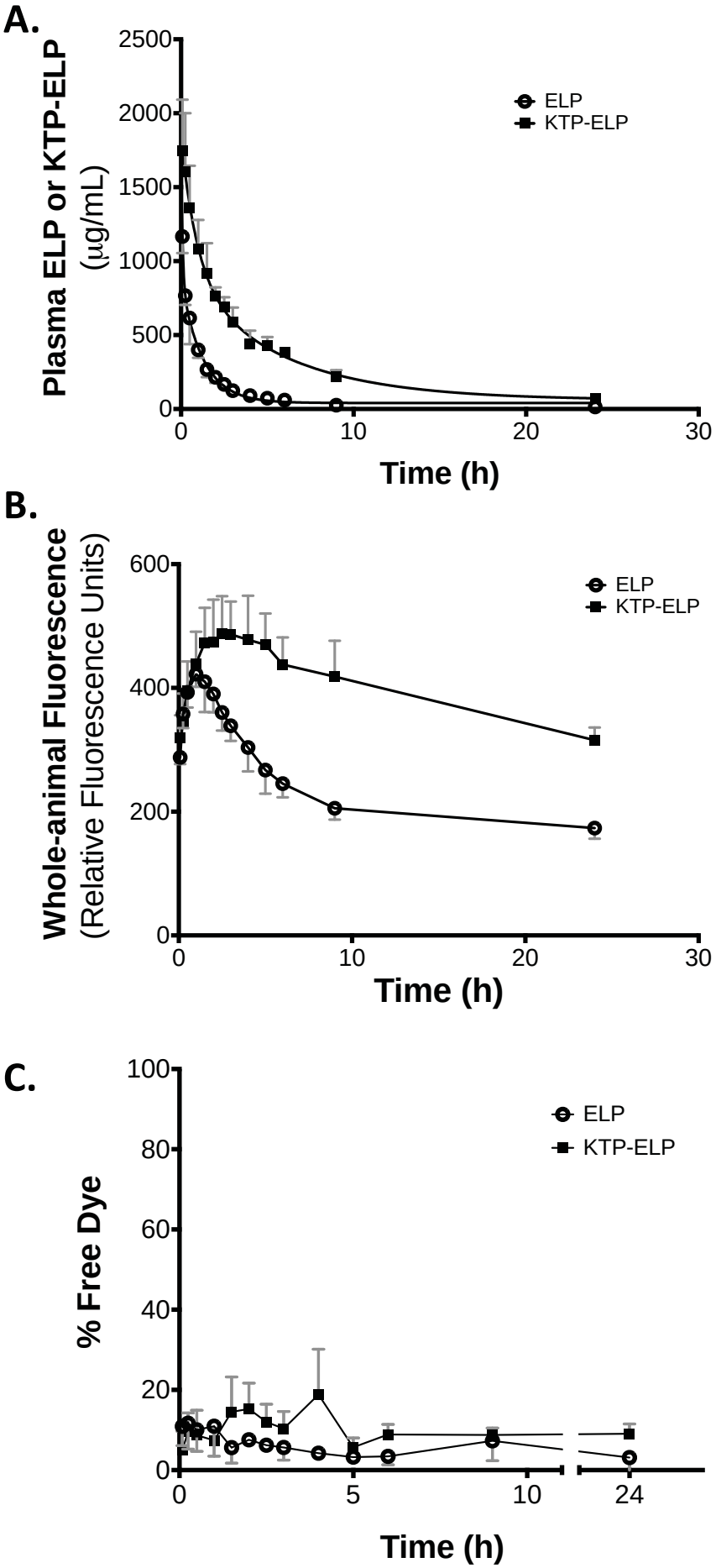
A.
Plasma ELP or KTP-ELP (μg/mL)
2500
2000
1500
1000
500
0
0
10
20
30
Time (h)
ELP
KTP-ELP
B.
Whole-animal Fluorescence (Relative Fluorescence Units)
600
400
200
0
0
10
20
30
Time (h)
ELP
KTP-ELP
C.
% Free Dye
100
80
60
40
20
0
0
5
10
24
Time (h)
ELP
KTP-ELP

Figure 4. (Revised)

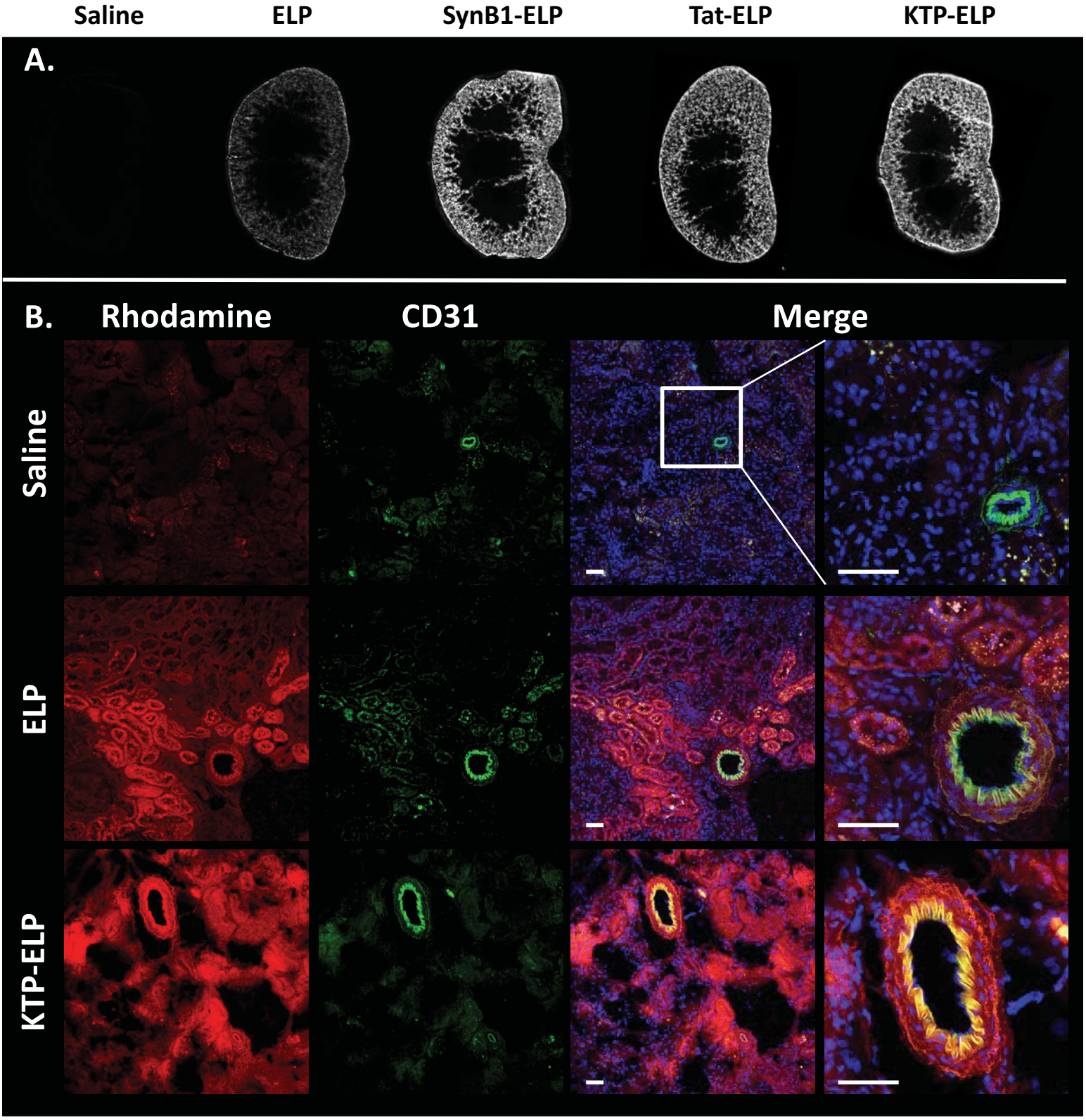

Figure 4. (Revised, continued)

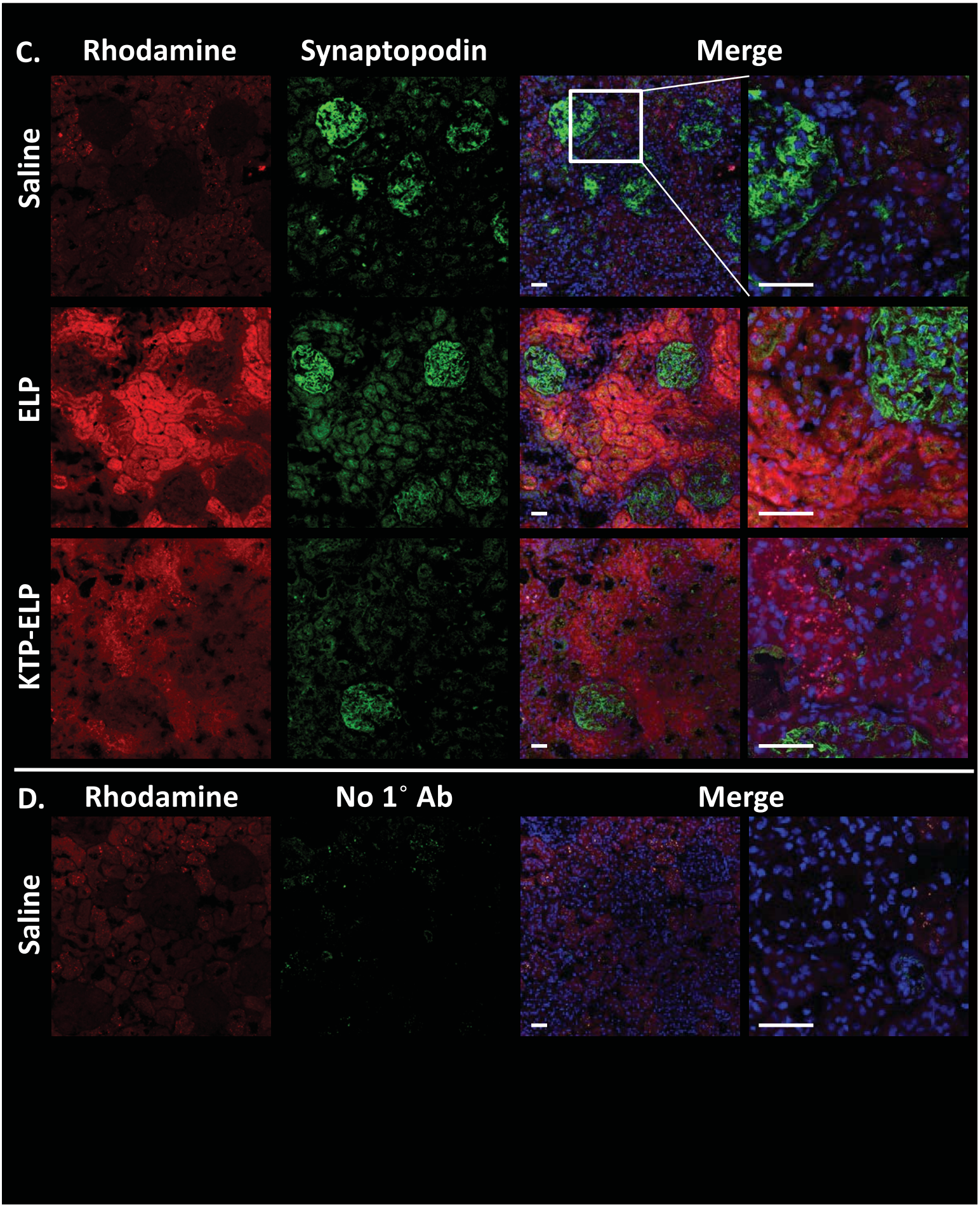

Figure 5. (New)

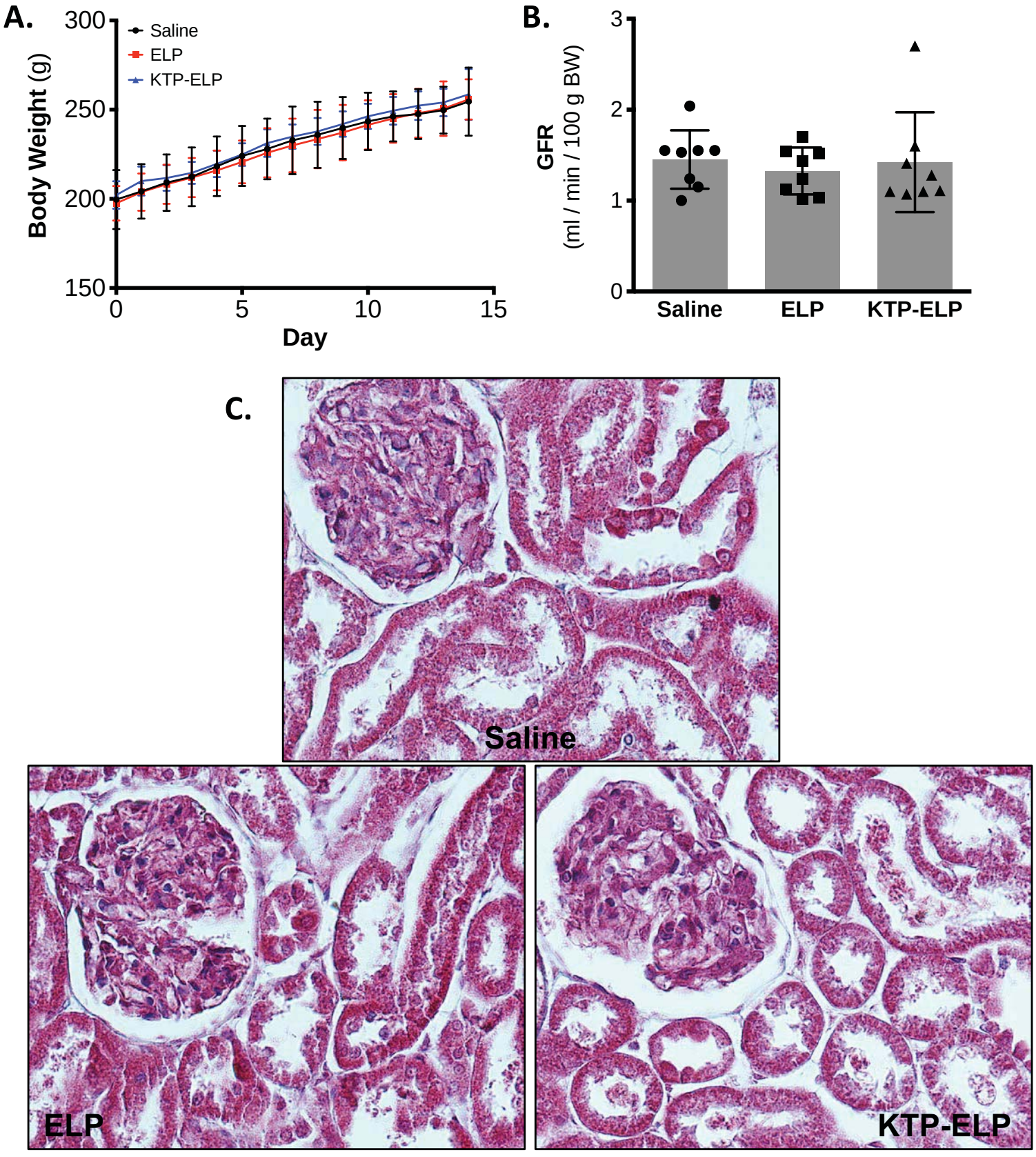
A.
Body Weight (g)
300
250
200
150
0
5
10
15
Day
Saline
ELP
KTP-ELP
B.
GFR
(ml / min / 100 g BW)
3
2
1
0
Saline
ELP
KTP-ELP
C.
Saline
ELP
KTP-ELP

Figure 6. (Revised)

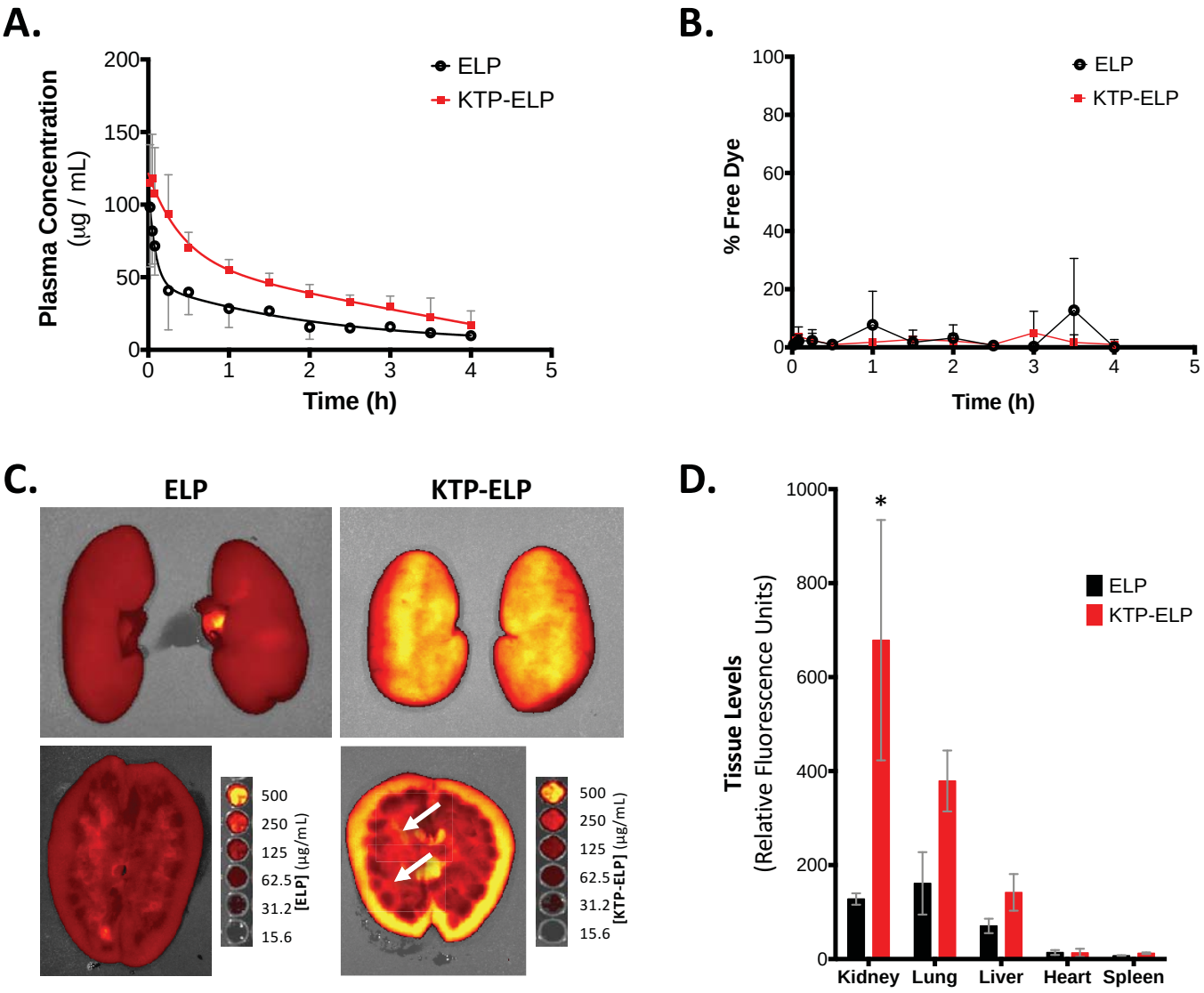

Figure 6. (Revised, Continued)

E.

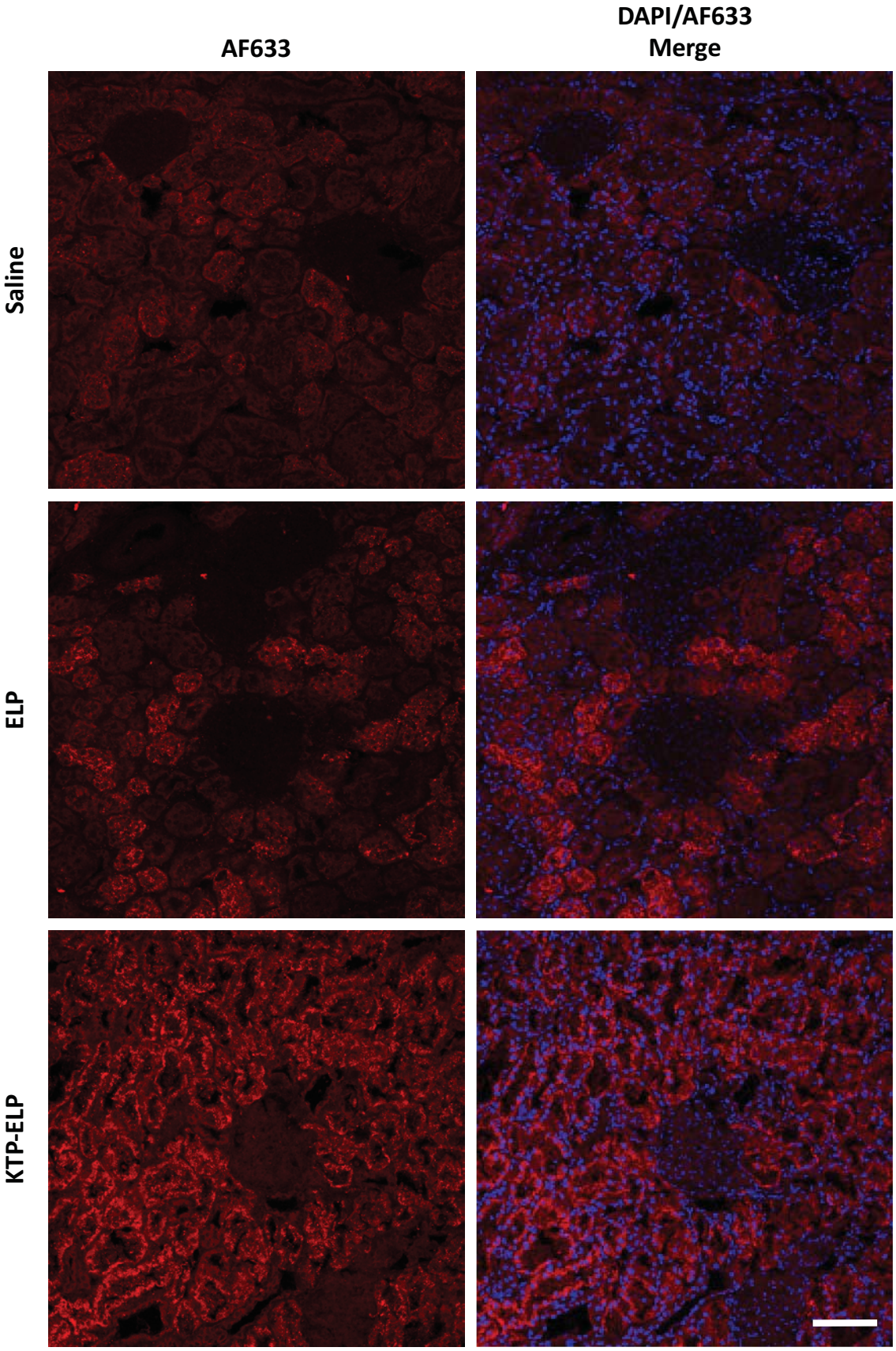

Figure 7.

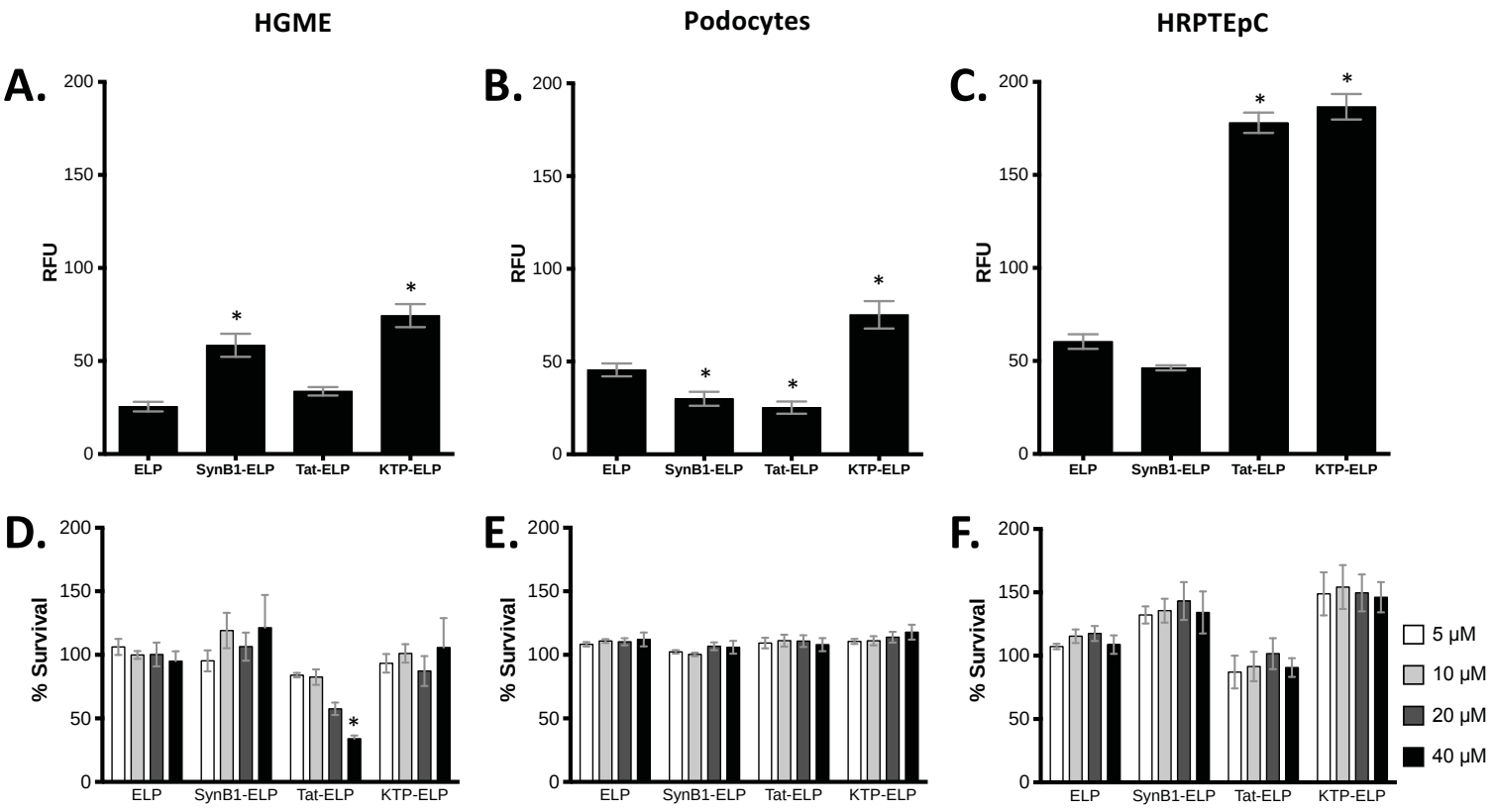
HGME
Podocytes
HRPTEpC
A.
B.
C.
RFU
200
150
100
50
0
*
ELP
SynB1-ELP
Tat-ELP
KTP-ELP
D.
E.
F.
% Survival
5 μM
10 μM
20 μM
40 μM